Journal of Computational Physics **173,** 433–454 (2001)
doi:10.1006/jcph.2001.6866, available online at http://www.idealibrary.com on IDEAL®

Application of a Hybrid Genetic/Powell Algorithm and a Boundary Element Method to Electrical Impedance Tomography

Chao-Tsung Hsiao,[1] Georges Chahine,[2] and Nail Gumerov[3]

Dynaflow, Inc., 10621-J Iron Bridge Road, Jessup, Maryland 20794
Web address: http://www.dynaflow-inc.com

Received January 13, 2000; revised March 7, 2001

An optimization method based on a genetic algorithm (GA) and a boundary element method is applied to solve an electrical impedance tomography problem. The scheme is applied to reconstruct highly irregular shapes and to image and count objects inside a host medium of different impedance. A Pareto multiobjective optimization method is applied to improve the performance of the GA. Comparisons between the GA and a calculus-based method for selected test problems show that the calculus-based method outperforms the GA in simple cases but that for more complex cases the GA reaches the correct solution whereas the calculus-based method does not. A hybrid scheme that we developed combining a calculus-based method and the GA is shown to be the most efficient and robust even when applied to the complex cases we tested. The sensitivity of the current scheme is evaluated in the presence of noise.

Key Words: electrical impedance tomography; genetic algorithm; boundary element method; inverse problem.

1. INTRODUCTION

Electrical impedance tomography (EIT) is a powerful imaging technique with a wide variety of applications requiring visualization of inaccessible objects or features. These include multiphase flows [1, 2], visualizing combustion [3], medical imaging [4], nondestructive evaluation of structures, determination of underground contaminant seepage, etc. In the EIT technique, the distribution of conductivity inside a domain is sought by applying specified currents (or voltages) at some parts of the interrogated domain surface and

[1] Senior Research Scientist, Dynaflow, Inc. E-mail: ctsung@dynaflow-inc.com.
[2] President, Dynaflow, Inc. E-mail: glchahine@dynaflow-inc.com.
[3] Senior Research Scientist, Dynaflow, Inc. E-mail: nail@dynaflow-inc.com.

0021-9991/01 $35.00

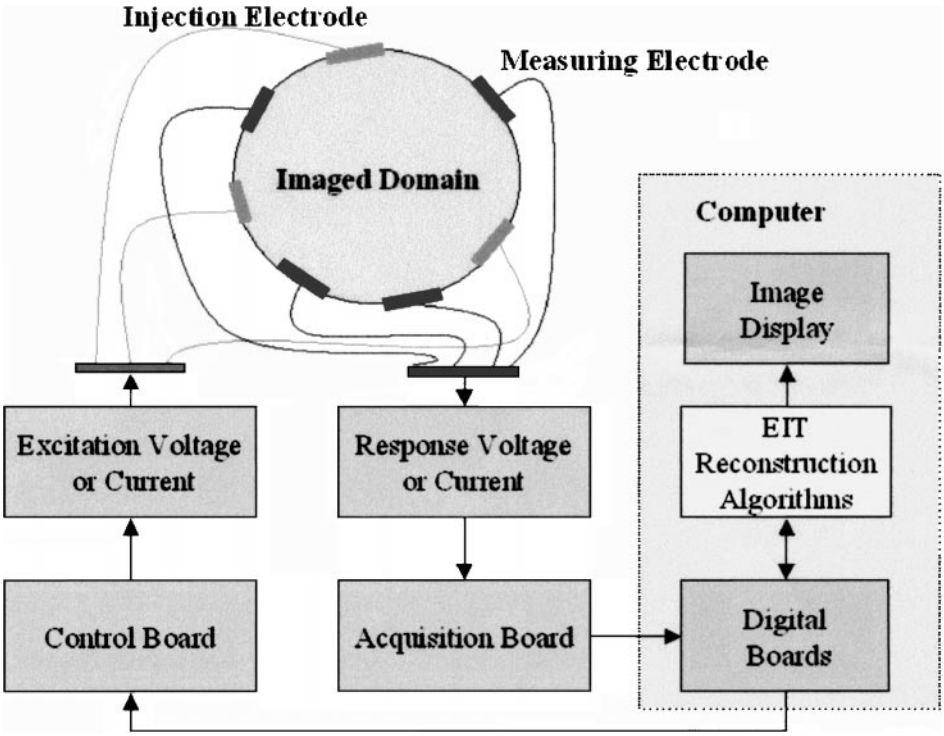

FIG. 1. Schematic of the electrical impedance tomography method.

performing measurements of the voltages (or currents) at other parts. The equations for the electric field then provide a relationship between the conductivity distribution inside the domain and the measured currents (or voltages). Solution of the resulting inverse problem then provides a map of the material distribution in the domain. A schematic of the EIT procedure is shown in Fig. 1. According to the user specifications, a control board arranges combinations of injection electrodes to form current (or voltage) patterns. The resulting voltages (or currents) are then measured at all combinations of measurement electrodes. The data on all voltages and currents over all injection and measurement electrodes are then stored using data acquisition boards, and used in the reconstruction procedure which is an inverse problem solution.

In EIT the equations are nonlinear and the inverse problem is solved by iterative techniques involving optimization procedures. Each iterative step requires solution of a boundary value problem, followed by the solution of a minimization problem. Schemes based on the finite element method [5, 6] are time consuming and require extensive computational resources, which make them difficult for practical usage, especially in 3D. We have developed [7–10] an efficient solution procedure based on the boundary element method (BEM) offering substantial speed-ups over conventional techniques. In our previous studies we have applied calculus-based optimization methods and a least squares approach, which combined the error evaluation function into a single objective function, to solve the inverse problem. These calculus-based methods such as the Powell method and the downhill simplex method were able to quickly reach the optimal solution for many cases we have studied. However, we encountered difficulties in robustness when the test cases became too complex, and when the desired global minimum was hidden among many local minima. Furthermore, the least

squares approach has the disadvantage of subsuming a detailed spatial error distribution into one all encompassing error function, which can have multiple local minimums.

Genetic algorithms (GAs), such as described by Holland [11] and Goldberg [12], are intelligent search methods based on a biological evolution mechanism concept and on Darwin's survival-of-the-fittest theory for solving complex problems. They are problem-independent and can process information generated at previous stages of a search process. They comprise concepts such as natural selection, quick exploration, and information collection in a design space. In contrast to most classical optimization methods, a GA requires no gradient information and results in simultaneous determination of multiple minima rather than a single local minimum. These characteristics make the GAs powerful tools for solving optimization problems. Since a GA has the characteristic of maintaining a population of solution and can search in parallel for many objectives, it inherently satisfies the requirement of seeking a Pareto optimal set in a multiobjective optimization problem. Therefore, it does not require combining multiple objectives into a single objective and can incorporate the concept of Pareto optimization [13] to solve an EIT multiobjective problem. This method allows taking into account all physical restrictions simultaneously and avoids the occurrence of cancellation effects between the various objectives as encountered in our previous studies [7–10].

The BEM approach that we have previously developed [14, 15] is applied here to solve the forward EIT problem in which for a given conductivity distribution we compute the currents (or voltages) at selected nodes resulting from input voltages (or currents) at other nodes. The inverse problem is then solved by applying optimization methods which minimize the error between the predicted and the measured currents (or voltages). In this study, two optimization schemes, the Powell method and a basic GA, are applied and their performances are compared for several test problems. To take advantage of the strengths of both methods, we then developed a hybrid scheme combining the GA and the Powell method to improve the performance of the optimization routine. All the example cases considered in the present study concern imaging the interior of a material of a given fixed conductivity (such as a metal or a liquid), which contains inclusions of zero or negligible conductivity (such as gas bubbles).

2. GOVERNING EQUATIONS

Consider an electrical impedance tomography problem where the voltage at selected points on the boundary is imposed. The current at boundary locations other than the electrodes is zero. At the electrodes the electrical current is measured in order to obtain the distribution of conductivity, σ, in the material. For a region Ω bounded by the surface S, the electric potential, ϕ, satisfies the following equation expressing electric charge conservation:

$$\nabla[\sigma(\nabla\phi)] = 0 \text{ in } \Omega. \tag{1}$$

With **n** being the unit normal vector to the boundary surface, ϕ is subjected to the following boundary conditions:

$$\begin{aligned} &\sigma\frac{\partial\phi}{\partial n} \text{ and } \phi \text{ known at the electrodes,} \\ &\frac{\partial\phi}{\partial n} = 0 \text{ at the rest of the boundary.} \end{aligned} \tag{2}$$

Unfortunately, a direct method for obtaining σ from these equations is not readily available. Instead, an inverse problem is solved through scanning and analysis of a wide space of guessed distributions of conductivity. For each guessed distribution of σ a forward problem is solved for the electric potential ϕ. Then, minimization of the error between the predicted and the measured values of ϕ on the boundary is sought in the space of guessed distributions of σ. The forward problem procedure solution is repeated as many times as necessary until satisfactory convergence is achieved.

In many applications, the domain to be imaged consists of regions of almost constant conductivity, σ_1, embedded in a continuous phase of another material of almost constant conductivity, σ_2 (e.g., a spatial multiphase distribution: solid, liquid, or gas). In this case the goal of the imaging is to determine the location of the interfaces S_{int}. Since the conductivity is practically constant within each of the materials, the field equation reduces to

$$\nabla^2 \phi_i = 0 \text{ in } \Omega, \quad i = 1, 2, \tag{3}$$

where $i = 1, 2$ represents each of the two substances. The boundary conditions at the outer surface are given by Eq. (2). In addition, the conditions of continuity of the potential and flux at the unknown interface(s) S_{int} can be written as

$$\phi_1|_{S_{\text{int}}} = \phi_2|_{S_{\text{int}}}, \quad \sigma_1 \frac{\partial \phi_1}{\partial n}\bigg|_{S_{\text{int}}} = \sigma_2 \frac{\partial \phi_2}{\partial n}\bigg|_{S_{\text{int}}}. \tag{4}$$

In these problems the forward problem consists of the solution of the Laplace equation in each medium using the coupling boundary conditions Eq. (4).

An additional important simplification arises if the interfaces to be imaged enclose materials of vanishing conductivity. Such situations are common in practice, e.g., in determining the distribution of air bubbles in a liquid or cracks in a structure. In this special case, the boundary conditions reduce to

$$\frac{\partial \phi}{\partial n} = 0 \quad \text{on } S_{\text{int}}. \tag{5}$$

Therefore, instead of solving the conductivity distribution, the objective of the problem is now to obtain the material interface, S_{int}.

3. NUMERICAL METHOD

The inverse problem in EIT can be addressed by a standard multistep, multidimensional optimization procedure, which consists of:

1. Parameterization: Parameterize the guessed conductivity distribution or shape of material interface.
2. Forward problem solver: Solve the Laplace equation corresponding to the guessed parameters.
3. Objective function: Evaluate the difference between the numerical solution of the guessed distribution and the actual measurement.
4. Optimization: Make a series of guesses of the parameters and obtain the final guess by minimizing the objective function.

3.1. Parameterization

One efficient way to make the iterative optimization routine successful is to parameterize the conductivity distribution, i.e., the conductivity distribution is represented in terms of a suitably selected descriptive basis function with a set of coefficients/parameters. Since the present algorithm is for imaging the interior of a material that consists of regions of constant conductivity, the parameterization can be selected to describe the shape and location of the internal objects. For example, the shape of an internal object in a 2D configuration can be represented by the sum of a series of N Legendre polynomials

$$S(\theta) = \sum_{k=0}^{N-1} \alpha_k P_k(\cos\theta - \theta_0), \tag{6}$$

where S is the distance from the origin selected to describe the object (x, y), and θ is the angle from a reference direction described by an additional parameter θ_0. P_k is the Legendre polynomial of order k, and α_k are N unknown parameters. This results in a total of $N + 3$ parameters for each object. A similar parameterization but using Fourier components was recently published [16]. Another possibility of describing the internal object is to parameterize the object with the coordinates of N points in addition to those at its center. Each point is at a distance r_k from the center of the object:

$$S(\theta) = r_k, \quad k = 1, \ldots, N. \tag{7}$$

This results in a total of $N + 2$ parameters for each object. For the relatively simple standard 2D problem of identifying cylindrical objects of vanishing conductivity inside a cylindrical container, each internal object can be parameterized by its radius, r, and the coordinate of its center. Similarly, for three-dimensional case of a container with internal regions consisting of spheres of vanishing conductivity, each internal sphere is parameterized by its radius, r, and the coordinate of its center (x, y, z).

3.2. Forward Problem Solver

To solve the forward problem at each iteration, a numerical scheme is required to solve the Laplace Eq. (3). In the current study we have selected the boundary element method for its great advantage of considerably reducing computational time especially for three-dimensional problems when compared to the finite element method. Indeed, by requiring discretization of only the boundary instead of the full domain, the BEM reduces the dimension of the problem by one and leads to orders of magnitude reduction in memory and CPU time requirements.

The boundary element method is based on an integral solution of the Laplace equation using Green's theorem, which can be written in the following form:

$$\int_\Omega (\phi \nabla^2 G - G \nabla^2 \phi)\, d\Omega = \int_S \mathbf{n} \cdot [\phi \nabla G - G \nabla \phi]\, dS, \tag{8}$$

where G is Green's function. Equation (8) transfers the domain integral into the surface integral and thus reduces the dimension of the problem by one. G is selected to be harmonic

everywhere but at discrete points such as the electrodes

$$G = \begin{cases} \log|\mathbf{x}-\mathbf{y}| & \text{in 2D,} \\ -\frac{1}{|\mathbf{x}-\mathbf{y}|} & \text{in 3D,} \end{cases} \tag{9}$$

where $\mathbf{x}$ is a point in Ω and $\mathbf{y}$ is a point on the boundary surface S. Substituting Eq. (9) into Eq. (8), we have

$$a\pi\phi(\mathbf{x}) = \int_S \mathbf{n}_\mathbf{y} \cdot [\phi(\mathbf{y})\nabla G(\mathbf{x},\mathbf{y}) - G(\mathbf{x},\mathbf{y})\nabla\phi(\mathbf{y})]\, dS, \tag{10}$$

where $a\pi$ is the angle in 2D (solid angle in 3D) under which the point $\mathbf{x}$ sees the rest of the domain. For formulations with smooth boundaries we have

$$a = \begin{cases} 2, & \mathbf{x}\in\Omega \quad \text{in 2D,} \\ 4, & \mathbf{x}\in\Omega \quad \text{in 3D,} \end{cases} \quad a = \begin{cases} 1, & \mathbf{x}\in S \quad \text{in 2D,} \\ 2, & \mathbf{x}\in S \quad \text{in 3D.} \end{cases} \tag{11}$$

To solve Eq. (10) numerically with the BEM, it is necessary to discretize the surface of all objects including the internal objects and the container into panels. In 2D we accomplish this by using P segments with N nodes along the boundary and by fitting cubic splines through the discrete points on the boundary. In 3D we use P triangular elements with N nodes on the boundary. As a result of this discretization, every surface integral evaluated at any field point $\mathbf{x}$ becomes a summation over all panels of the influence of singularity distributions over each individual panel. This enables us to write Green's identity in the form

$$a\pi\phi(\mathbf{x}) = \sum_{k=1}^{P} \int_{S_k} \left(\phi(\mathbf{y}) \frac{\partial G}{\partial n}(\mathbf{x},\mathbf{y}) - G(\mathbf{x},\mathbf{y}) \frac{\partial \phi}{\partial n}(\mathbf{y}) \right) dS_k. \tag{12}$$

To evaluate the integrals given in Eq. (12), it is necessary to prescribe the variation of ϕ and $\partial\phi/\partial n$. For this problem, we assume that these quantities vary continuously over a panel and can be described by the surrounding nodes. By applying a cubic spline interpolation in 2D and a linear Lagrangian interpolation in 3D for each panel S_k, each elementary integral can be written as a linear combination of ϕ or $\partial\phi/\partial n$ evaluated at the surrounding nodes. The performance of integration (including special cases that are singular when the collocation node lies in the interval of integration) is an involved process, and details can be found in our previous studies [14, 15]. With the integration over each panel performed, the discreized Eq. (12) can be expressed as

$$a\pi\phi_j = \sum_{k=1}^{P} \sum_{i=1}^{m} \left[B_i^k \phi_i^k - A_i^k \left(\frac{\partial\phi}{\partial n} \right)_i^k \right], \quad j = 1, N, \quad m = \begin{cases} 2, & \text{in 2D,} \\ 3, & \text{in 3D,} \end{cases} \tag{13}$$

where ϕ_i^k and $\partial\phi/\partial n_i^k$ are the potential and its normal derivative at node i of panel k, and A_i^k and B_i^k are influence coefficients obtained from elementary integration.

Following a collection approach in which the contributions due to the same node are summed up, Eq. (13) can be rewritten as

$$a\pi\phi_j = \sum_{i=1}^{N} \left[\bar{B}_i \phi_i - \bar{A}_i \left(\frac{\partial\phi}{\partial n} \right)_i \right], \quad j = 1, N, \tag{14}$$

where $\bar{A}$ and $\bar{B}$ are the altered influence coefficients due to summation of the same node. It is noted that the collection approach transfers the panel contribution in Eq. (13) to the node contribution in Eq. (14). Equation (14) can be expressed in a matrix form as

$$(a\pi \mathbf{I} + \bar{\mathbf{A}})\phi = \bar{\mathbf{B}}\frac{\partial \phi}{\partial n}, \tag{15}$$

where $\mathbf{I}$ is an $N \times N$ identity matrix, and $\bar{\mathbf{A}}$ and $\bar{\mathbf{B}}$ are $N \times N$ influence coefficient matrices. With $\partial\phi/\partial n$ known on all boundary nodes, Eq. (15) is a linear system of N equations and can be readily solved for N unknowns of ϕ, using classical methods such as LU decomposition and Gauss elimination.

3.3. Objective Function

In the current study, the error between the predicted solution and the measured data is given by

$$e_l^k = \hat{\phi}_l^k - \phi_l^k, \quad l = 1, \ldots, M_E, \quad \text{and} \quad k = 1, \ldots, N_E, \tag{16}$$

where $\hat{\phi}_l^k$ and ϕ_l^k are the measured and predicted values of the potential at electrode l for the current injection configuration k, M_E is the number of measuring electrodes, and N_E is the number of experiments. We thus have $M_E \times N_E$ measures of the error, e_l^k.

Previously [7–10], we applied a least squares approach to construct a single objective function using the following root mean square (RMS) error function:

$$f = \sqrt{\sum_{k=1}^{N_E}\sum_{l=1}^{M_E}\left(\hat{\phi}_l^k - \phi_l^k\right)^2}. \tag{17}$$

One shortcoming of performing the minimization using this single objective function is that all the physical information available from each experiment at all electrodes are added into a single objective function. However, the physical information of the error distribution may have a spatial pattern that could be advantageously used. This information is useful for an optimization routine to better characterize the predicted solutions so that the convergence rate can be enhanced. To better use this physical information, a multiobjective approach is therefore applied in the current study. To demonstrate this we apply the multiobjective approach to a two-dimensional cylindrical container. If there are n_{obj} objective functions applied, then the objective functions for are constructed as follows:

$$\begin{aligned} f_i &= \sqrt{\sum_{l=M_1}^{M_2}\sum_{k=1}^{N_E}\left(\hat{\phi}_l^k - \phi_l^k\right)^2 + \sum_{l=M_1+M_E/2}^{M_2+M_E/2}\sum_{k=1}^{N_E}\left(\hat{\phi}_l^k - \phi_l^k\right)^2}, \\ M_1 &= \frac{(i-1)M_E}{2n_{obj}} + 1, \quad M_2 = \frac{iM_E}{2n_{obj}}, \quad i = 1, \ldots, n_{obj}. \end{aligned} \tag{18}$$

Based on Eq. (18), the objective functions will be formed each by adding the errors from two noncontiguous quarters on the container surface for a two objective approach. However, for

both single objective and multiobjective approaches the convergence speed is represented by computing the normalized root mean square error

$$\varepsilon = \frac{\sqrt{\sum_{k=1}^{N_E}\sum_{l=1}^{M_E}\left(\hat{\phi}_l^k - \phi_l^k\right)^2}}{\sqrt{\sum_{k=1}^{N_E}\sum_{l=1}^{M_E}\left(\hat{\phi}_l^k\right)^2}}. \tag{19}$$

In solving inverse problems, it is quite important to constrain the solution using a priori information to mitigate any ill-posed character of the problem. For example, one can use obvious geometric constraints such as the fact that the internal objects cannot overlap or intersect the container, or that their size is bounded by known minimum and maximum values. To cope with the constrained problem, the objective function is modified to return artificially very large values when presented with unrealizable configurations. These are made more or less large according to the degree of violation. In addition, for calculus-based methods the error gradient vector is set to the unit vector in the direction that leads away from the error.

3.4. Optimization Routines

The success of developing an efficient and robust EIT software highly relies on the optimization routine. Here, several optimization routines, including a calculus-based method, a random search algorithm, and a hybrid scheme, are applied and compared for several test problems.

3.4.1. *Powell Direction Set Method*

The first method used here is the Powell direction set method also known as the Davidon–Fletcher–Powell method. The Powell method applied in the current study is the version described in [17, 18] in which an initial guess and a set of independent search directions are provided to the program. In each iteration the method serially performs a sequence of line minimizations along the various directions in the space of parameters. At the end of each iteration the method replaces one of the original directions with the line joining the starting and ending points. Care is taken to ensure that the directions remain linearly independent. The iteration is terminated when either the convergence rate or the error between the predicted and the exact solutions are smaller than prescribed values. This version of the Powell method has been successfully applied to the EIT problem [7–10] and widely applied to other optimization and minimization problems (see for instance [19–22]). Although there are many other implementations of the Powell method such as described in [23, 24], the current study does not intend to include a comparative study of the merits of each of these implementations.

3.4.2. *Simple Genetic Algorithm*

An implementation of a GA begins with the selection of a population of members. Each member in the population represents a guessed solution of the problem i.e., a set of parameters describing the shape and position of the sought objects). The GA identifies each member by encoding it as a chromosome (typically, bit strings). The objective function described above is an evaluation function that plays the role of the environment, rating the members

in terms of their fitness. This is the mechanism applied to select good quality members of a population to reproduce the population of the next generation. The reproduction procedure is such that well-fit members are given more chance to reproduce than members which are poorer performers. The process of evolving from a given population to the next population constitutes one generation in the execution of a GA. The basic implementation of a simple genetic algorithm can be summarized as follows [12]:

Step 1, Initialization: Create an initial random population of members and identify each member with a chromosome (bit strings).

Step 2, Evaluation: Evaluate the fitness of each member in this population based on the corresponding value(s) of the objective function(s).

Step 3, Selection: Select two parent chromosomes from the current population to reproduce offsprings. The selection process is stochastic with the high fitness members being more likely to be selected.

Step 4, Reproduction (crossover): Generate two offsprings from two parent chromosomes by exchanging bit strings.

Step 5, Mutation: Apply a random modification of the bit strings to each offspring with a small probability.

Step 6, Iteration: Repeat Steps 2, 3, and 4 until the number of offsprings in the new population is the same as the number of parents in the old population.

Step 7, Iteration: Go to Step 2.

To improve the search process of the global optimum, an additional operator, elitism, was implemented. Elitism forces the best individual to always be selected for reproduction until someone comes along which is stronger to take over its place. After the population is generated, the GA checks to see if the best parent has been replicated. If not, then a random individual is chosen and the chromosome set of the best parent is mapped into that individual.

To adapt the GA to the current problem, each guessed distribution of the internal objects is identified by a binary chromosome. Since each internal object is parameterized either by the coordinates of its center and a series of Legendre polynomials or by the distance of the surface nodes from its center, each set of parameters $p_i (i = 1, K)$ is represented in the genetic structure. This means that each object has K independent variables, which correspond to K genes represented as a bit string of total length M. Each parameter has its own bit string of length L_i $(i = 1, K)$. If there are N objects inside a material, then each possible distribution of internal bodies is represented as a binary chromosome of length $M \times N$. Figure 2 shows an example of the representation of a chromosome. Since each bit string represents an integer J while each variable is given by a real value a, we chose a mapping between the real value a $(p \leq a \leq q)$ and the integer J $(0 \leq J \leq L - 1)$ such that the integer interval $[0, 2^{L-1}]$ is mapped onto the real interval $[p, q]$.

3.4.3. *Multiobjective Genetic Algorithm with Pareto Optimization*

Instead of smearing all the information into a single objective, we implement a multi-objective optimization method incorporating the concept of Pareto optimal set [13] to exploit the knowledge of spatial distribution of the error. A *Pareto optimal set* can be described as follows: A point in the objective variables space is Pareto optimal if one cannot find another point which is better with respect to at least one objective without

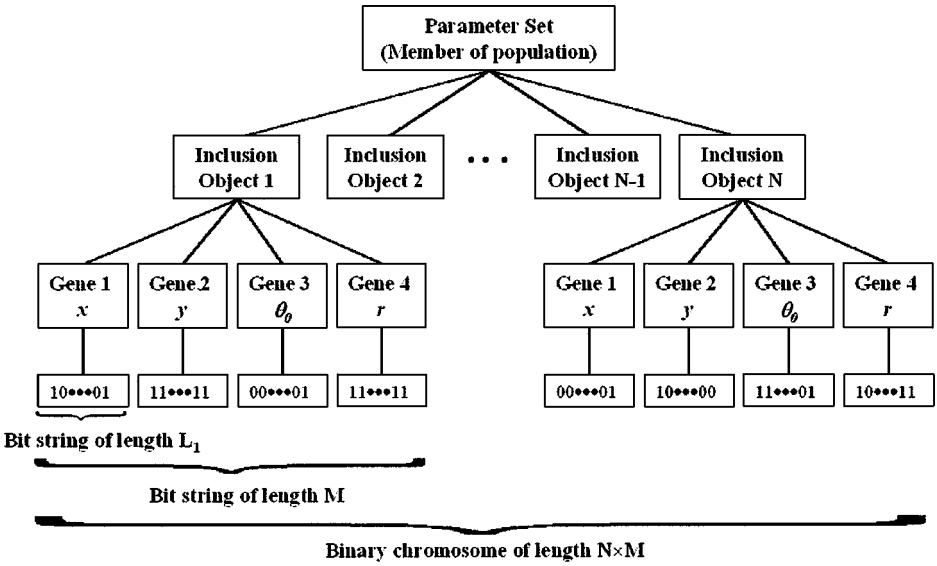

FIG. 2. A sketch showing conversion of the parameter set describing a guessed solution into a chromosome bit string.

sacrificing with respect to at least one other objective. This means that the Pareto optimum gives a set of nondominated points for which no objective can be improved without degrading at least one other objective. Searching for the Pareto optimal set (a group of solutions) is the goal for solving the multiobjective problem. Once the Pareto optimal set is determined, the decision maker is able to define the optimal solution from the Pareto optimal set according to other nonmodeled criteria. Since the GA has the characteristic of maintaining a population of solutions and can search in a parallel manner for many nondominated solutions, the GA inherently satisfies the requirement of seeking a Pareto optimal set in a multiobjective optimization problem. Therefore, we use a Pareto GA similar to that suggested by Cheng and Li [13] to solve the current problem.

The current Pareto GA is constructed by revising the simple GA. Unlike the simple GA, where the fitness function is determined directly from the objective function, in the Pareto GA the fitness function of each individual is determined from its ranking. To achieve this goal a ranking procedure [12] is used. At each generation nondominated solutions are selected and assigned rank 1. From the remainder of the population, nondominated solutions are identified and assigned rank 2. This process continues for rank 3, 4, and so on until the entire population is ranked. After the whole population is ranked, the fitness value of points in rank i can be determined by the following [12]

$$F_i = \frac{M_p(N_r - i + 1)}{\sum_{i=1}^{N_r}(N_r - i + 1)N_i}, \tag{20}$$

where M_p is the population size, N_r is the highest rank of the population, N_i is the population size of rank i, and F_i is the fitness of a point ranked i.

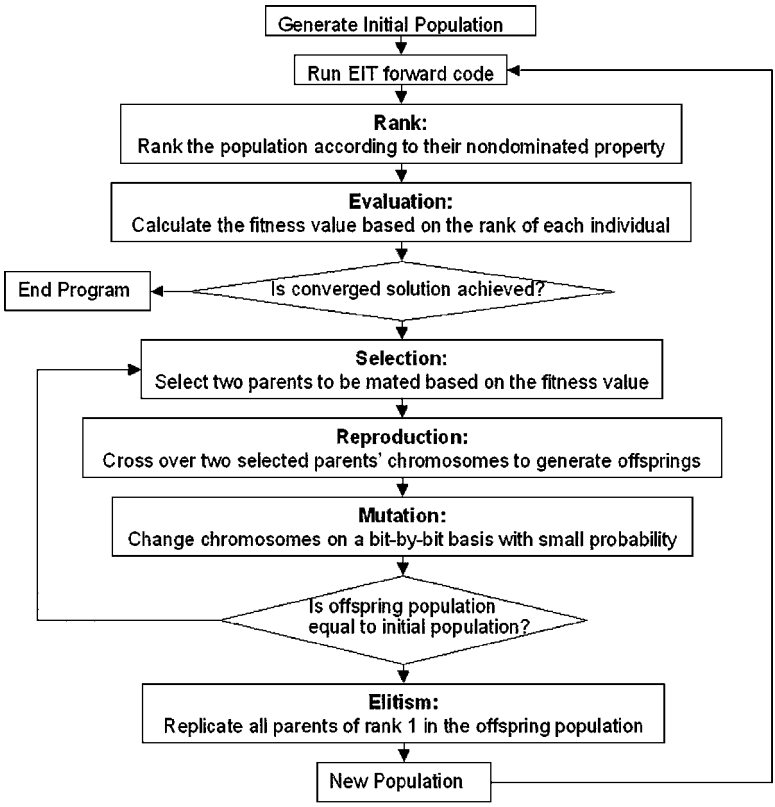

FIG. 3. A flow chart for the Pareto optimization EIT multiobjective problem using a genetic algorithm.

To improve the search process of the Pareto optimal set, the current Pareto GA also uses the elitism operator. However, instead of ensuring only reproduction of members with the highest fitness, the elitism technique of the Pareto GA ensures that all members with rank 1 appear in the next generation. Figure 3 illustrates the multiobjective GA optimization scheme that we developed for the EIT problem.

3.4.4. *Hybrid Optimization Scheme*

Although the GA is recognized as a highly robust optimization scheme, the slow convergence rate has prevented the GA from becoming practical in many applications. On the other hand, the calculus-based methods are known for their fast convergence speed but they are very sensitive to the initial guess of the solution. Therefore, we exploited in the current EIT problem the benefit of combining the Powell method and the GA. The proposed hybrid scheme starts with the GA. The Powell method is turned on after a prescribed number of generations, N_g, is iterated. The connection between the GA and the Powell method is made by choosing the best solution from the current population to be the initial guess for the Powell method. When the convergence rate of the Powell method reaches a plateau without reaching the criterion for global minimum, then the optimization routine returns to the GA which is made to iterate again for N_g generations, and the process is repeated until the global minimization criterion is reached.

4. RESULTS AND DISCUSSION

4.1. Numerical Aspects

In order to test the proposed method, we start by using the forward problem solver to generate a set of ideal "experimental" data for a given distribution of internal objects. For the two-dimensional case the ideal "experimental" data is collected at 20 electrodes on the container surface. Similarly, the container and each internal objective is discretized using 20 panels.

Several parameters of the GA basic operators need to be determined for optimal performance. These parameters include the mutation probability, the crossover probability, the discretized size of the parameters, and the population size. As suggested by Goldberg [12] the mutation probability was set to the inverse of the population size and the crossover probability was set to 0.6. The solution accuracy of the GA depends heavily on the length of the chromosome because a longer bit string yields a smaller discretized size of the parameters. The smaller the discretized size of the parameters is, the more accurate the solution that can be obtained. Decreasing the discretized size of the parameters, however, increases the search domain and leads to a slower convergence process. Therefore, a compromise is necessary. In the present study, the discretized size was chosen to be less than 2% of the characteristic length, which was selected here to be the smallest projected dimension of the imaged domain.

The determination of the population size depends on the complexity of the problem, e.g., number of internal objects and complexity of object shapes. The more complex the problem is, the larger the population size should be. For a simple two-dimensional case, such as one or two internal objects with circular shape, a population with 50 individuals is sufficient. However, for a complex case a small population size may lead the GA to converge to a local minimum. To demonstrate the importance of the population size in a complex case, two different population sizes, 50 and 100 were used for a two-dimensional four-circle case with one of the circles being relatively small and somewhat hidden among the other larger circles. Both cases were used to conduct a search until the convergence rate reached a plateau. The converged solutions for using 50 and 100 individuals are compared to the exact solution and shown in Fig. 4. It is seen that with a smaller population size the GA did not converge to the global minimum while with a larger population size the GA predicted the solution quite well.

4.2. Comparison between Single and Multiobjective Approaches

Although it is expected that keeping spatial information in the error functions will improve the convergence rate, increasing the number of objective functions also slows down the search process due to the overhead of keeping all first-rank individuals. To test the efficiency of using more than one objective function for our current problem, we tested both single and two objective approaches for two-dimensional three-circle cases. Comparison of convergence rates for these approaches is shown in Fig. 5. It is found that the two objective approach reached the convergence criterion faster than single objective approach. Similar comparative results were also observed for the two-dimensional four-circle case.

4.3. Comparison between Powell Method and Genetic Algorithm

We conducted systematic comparisons between our implementation of the Powell method and of the GA in two- and three-dimensional cases. We found that in our case the

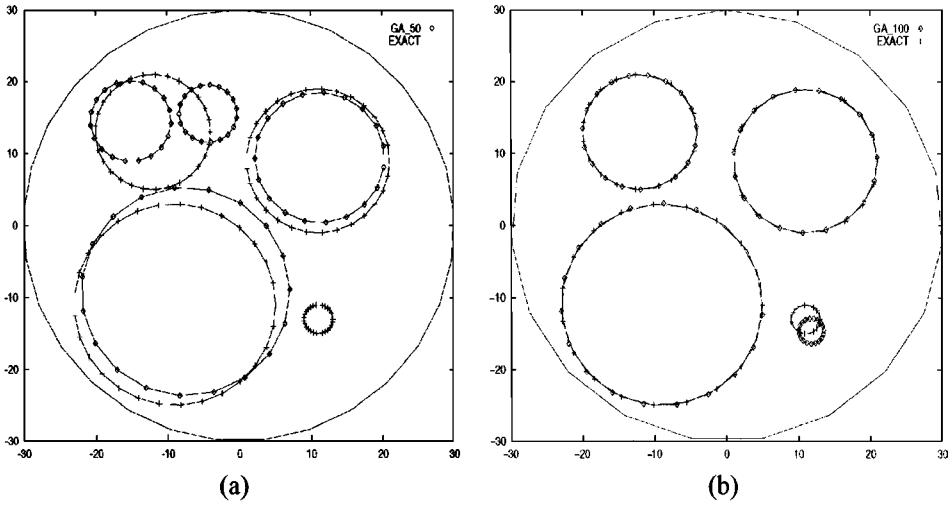

FIG. 4. The exact and reconstructed solutions of four-circle case using the genetic algorithm for population size of (a) 50 and (b) 100.

calculus-based Powell method outperforms the GA in simple cases, as shown by comparison of the convergence histories for both one- and two-circle 2D cases in Fig. 6. Both the Powell method and the GA converged very well to the exact solution. The Powell method, however, reached the exact solution much faster than the GA for both cases.

To increase the problem complexity, the number of circles was increased to 3 with 2 of them very close to each other. Figure 7 shows the exact solution and the converged solutions of the Powell method and the GA in this case. A comparison of the convergence histories for

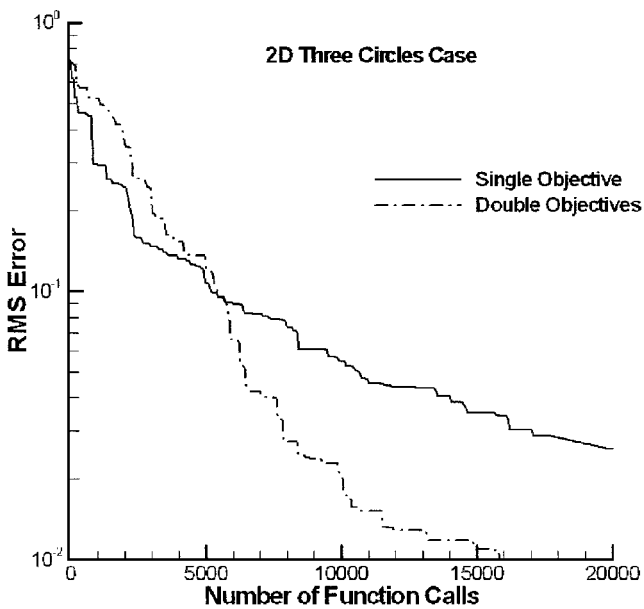

FIG. 5. The convergence histories of single and two objective approaches for the 2D three-circle case.

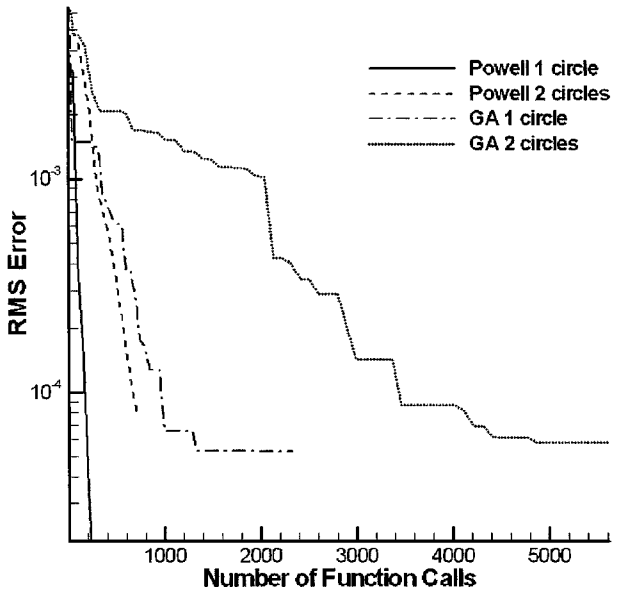

FIG. 6. Comparison of the convergence histories of the Powell method and the genetic algorithm for the one- and two-circle cases.

the Powell method and the GA is shown in Fig. 8. It is seen that in this case the Powell method converged to a local minimum while the GA correctly found the global minimum. Although we tested several different initial guesses for the Powell method, none of them reached the exact solution. Similar comparisons were also conducted for two spheres (eight parameters)

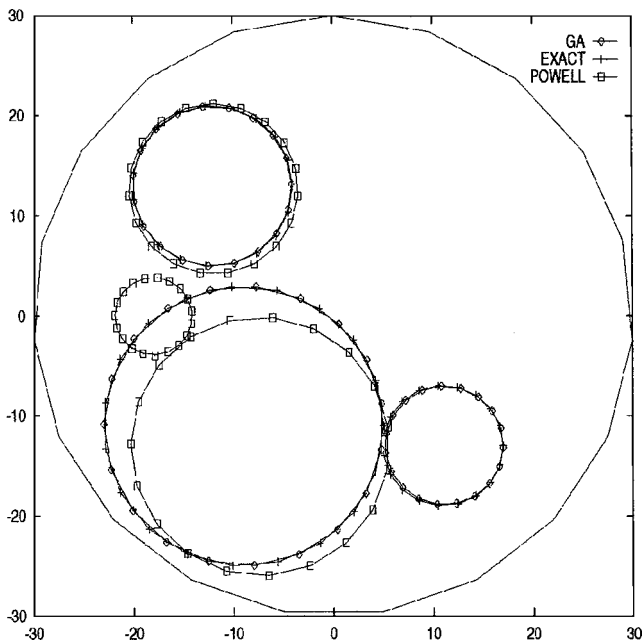

FIG. 7. Comparison of the exact and reconstructed solutions using the Powell method and the genetic algorithm for the three-circle case.

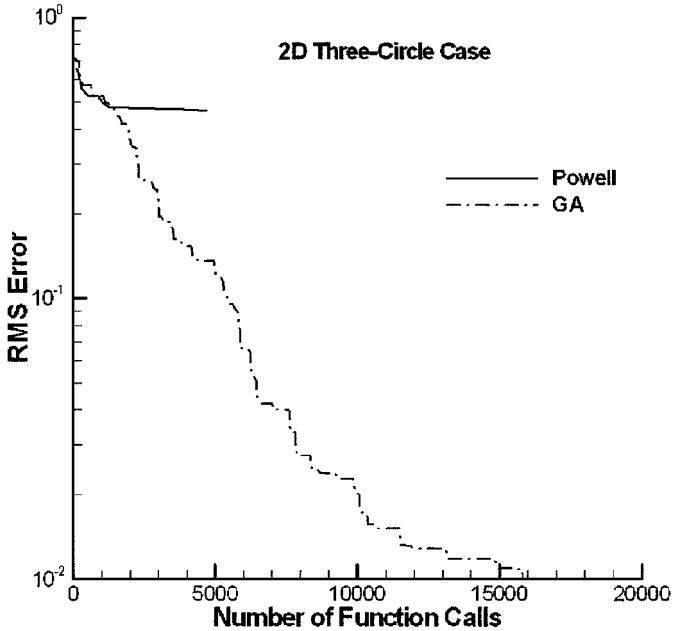

FIG. 8. Comparison of the convergence histories of the Powell method and the genetic algorithm for the three-circle case.

in the three-dimensional case. Figure 9 shows the exact solution and the converged solution of the Powell method for the two-sphere case. It is seen that after convergence one of the spheres is still offset from the exact solution. In this case the GA still preformed very well and the converged solution ended indistinguishable to the eye from the exact solution for

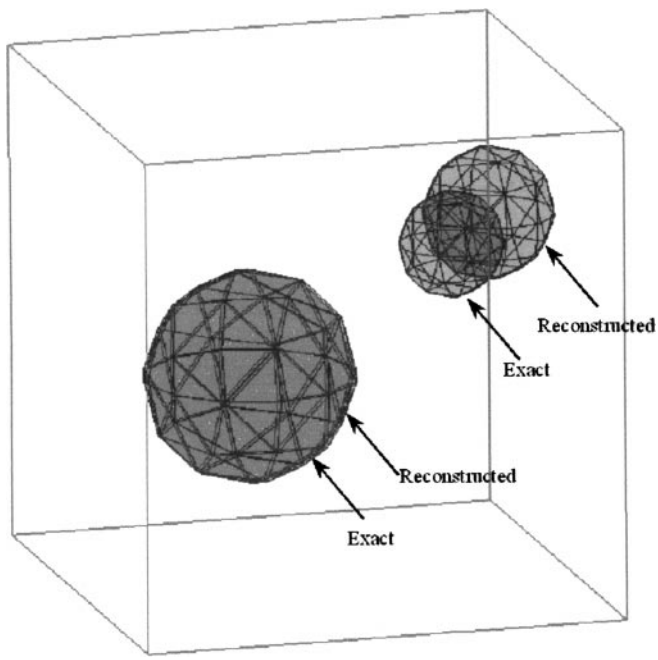

FIG. 9. Exact and reconstructed solutions using the Powell method for the two-sphere case.

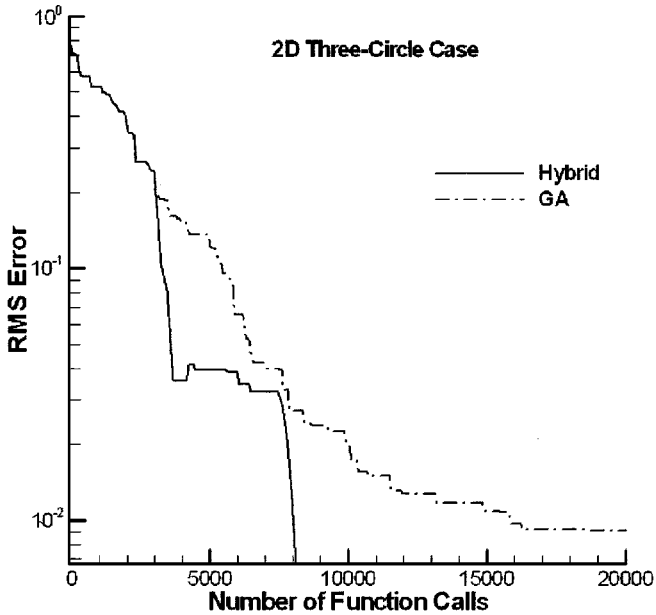

FIG. 10. Comparison of the convergence histories between the genetic algorithm and the hybrid scheme for the 2D three-circle case.

both spheres. It is important to note that there are different implementations of the Powell method. Although the version of the Powell method applied in the current study fails to reach the global minimum, there may be other versions of the Powell method that may improve the result. Nevertheless, searching for the best version of the Powell method was not within the scope of the current study.

4.4. Comparison between the Genetic Algorithm and Hybrid Scheme

To demonstrate how the hybrid scheme can improve the convergence rate, we applied it to solve the three-circle case shown earlier with $N_g = 50$. The comparison of convergence histories between the GA and the hybrid scheme is shown in Fig. 10. It is seen that strong improvement is achieved when the Powell method is first turned on after 50 generations (3000 function calls). The hybrid method reduces the error faster than the GA until the convergence rate reaches a plateau. The iteration process then returns back to the GA and continued for another 50 generations. When the Powell method is turned on again, a second significant drop in the RMS error is observed and the global minimum is reached. It is noted that the procedure can be further optimized by modification of the procedure parameters (e.g., number of generations before switching). The improvement in convergence rate is more significant when the studied case is more complicated. For very complex cases, the GA may stop converging before reaching the global minimum because the homogeneity of the chromosomes may be reached first. In this case, the improvement of the solution will only rely on the mutation and become a very slow process. As shown in Fig. 11, for a two-dimensional six-circle case the convergence rate of the GA reached a plateau while the hybrid scheme with $N_g = 100$ converged very fast. The final solutions of both schemes are also compared with the correct answer and are shown in Fig. 12.

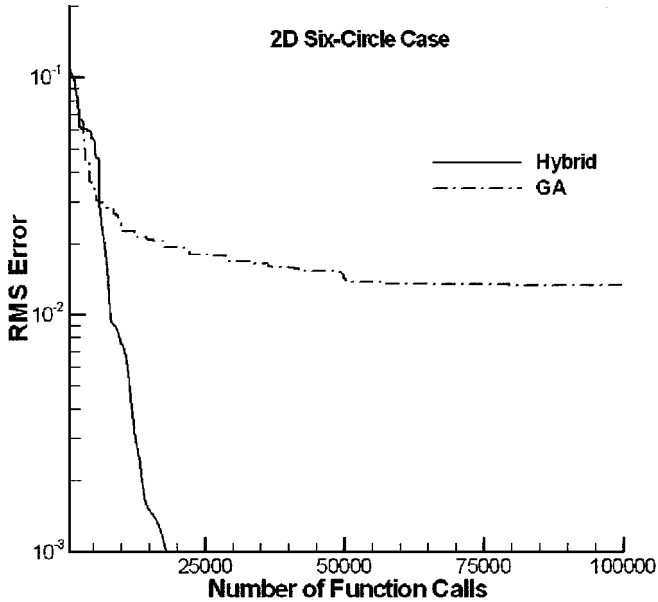

FIG. 11. Comparison of the convergence histories between the genetic algorithm and the hybrid scheme for the 2D six-circle case.

4.5. Study of Parameterization

To demonstrate the flexibility of the current scheme, different parameterization methods were applied to study more complex cases. Figure 13 shows that the exact and reconstructed solutions using five Legendre polynomials for a configuration with two irregular shaped objects. It is seen that the reconstructed solution matches the exact solution quite well except in the very fine details of the shape. However, to obtain a satisfactory reconstructed solution for more irregular shapes, such as an object with many sharp angles, using the Legendre polynomials may not be adequate. Figure 14 shows the exact solution and the reconstructed

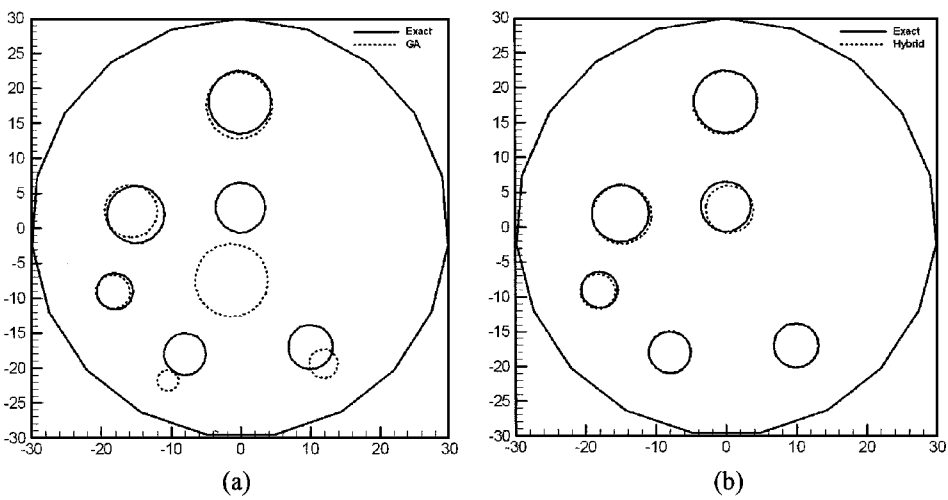

FIG. 12. Comparison of the exact and reconstructed solutions (a) the genetic algorithm and (b) the hybrid scheme for the six-circle case.

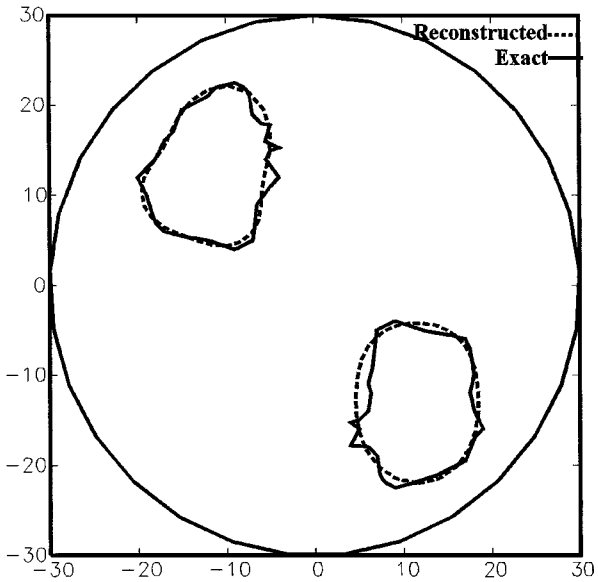

FIG. 13. Comparison between exact and reconstructed solutions using five degrees of Legendre polynomial parameterization for two irregular objects.

solution using the point parameterization with 32 parameters as described in Eq. (7) for a star-like object. Despite a less than perfect match, the overall characteristics of the object such as the location, area, and presence of large spikes are well reconstructed.

The examples shown so far assumed that the number of internal objects is known. In practical applications, however, the number of internal objects is usually unknown. To make the current EIT software more flexible, we added an extra parameter to each internal object in addition to the parameters describing the position and shape. This extra parameter

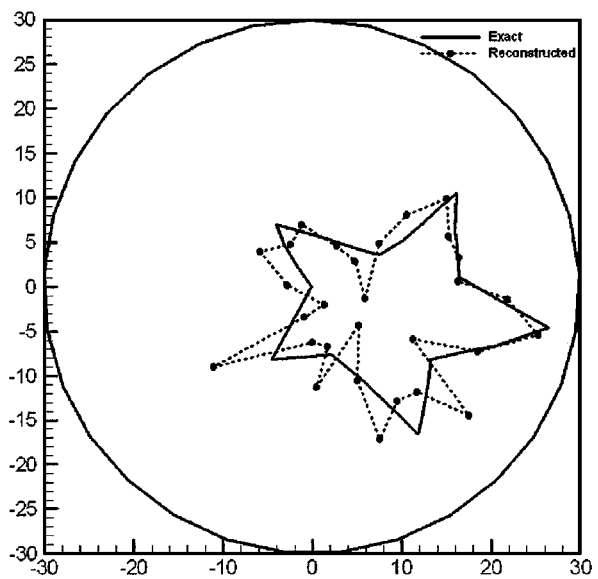

FIG. 14. Comparison between exact and reconstructed solutions using point parameterization with 32 parameters for one irregular object.

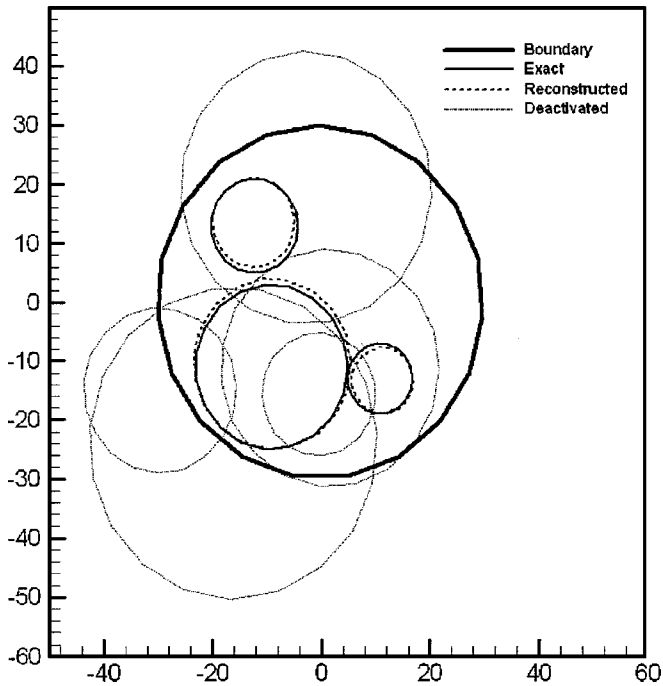

FIG. 15. Comparison between exact and reconstructed solutions obtained using an initial guess of 10 circles to reconstruct the three-circle case.

is binary and activates the internal object if equal to 1 and deactivates it if equal to 0. With this extra on/off parameter, one can reconstruct the image without knowing the exact number of internal objects. Figure 15 shows the reconstructed solution which was obtained by using an initial guess of 10 circles to reconstruct the three-circle case. The circles with dotted lines shown in Fig. 15 were deactivated by the algorithm during the convergence procedure.

4.6. Study of Noise Influence

An important question is to what extent the current scheme is sensitive to errors in the experimental measurements. The examples shown so far assumed experimental data with no errors. To determine the sensitivity to inherent experimental errors, a series of simulations were conducted for the two-dimensional three-circle case. Three different degrees of accuracy in experimental data were represented by imposing random changes in $\hat{\phi}_l^k$ with maximums 10, 20, and 40%. Since the altered data does not necessarily satisfy the Laplace equation, the error between the altered data and the numerical prediction is not expected to converge to zero. To determine the influence of noise, the reconstructed solution is compared to the exact solution by computing the differences in the parameters using the RMS value

$$\varepsilon_p = \frac{\sqrt{\sum_{i=1}^{3}\sum_{j=1}^{3}\left(\hat{p}_i^j - p_i^j\right)^2}}{\sqrt{\sum_{i=1}^{3}\sum_{j=1}^{3}\left(\hat{p}_i^j\right)^2}}, \tag{21}$$

where $\hat{p}_i^j$ and p_i^j are the parameters of the exact solution and the reconstructed solution,

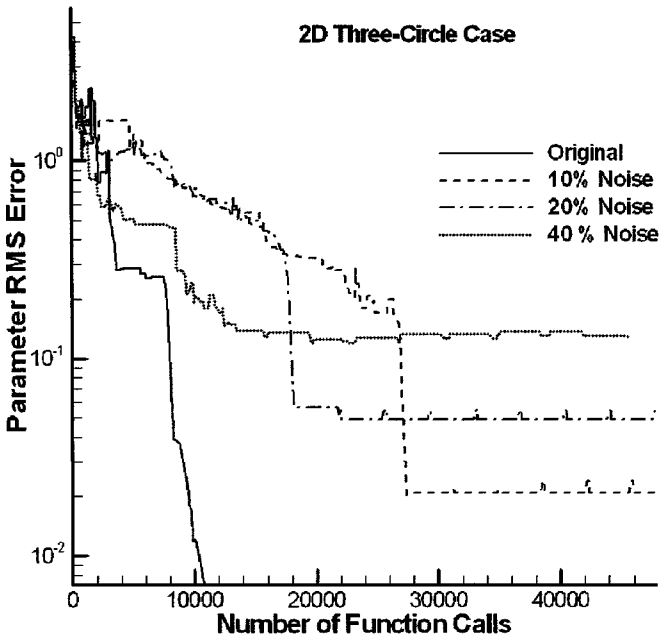

FIG. 16. Comparison of convergence histories of parameter RMS errors for different degrees of noise.

respectively. For the two-dimensional three-circle case, each circle has three parameters, x, y, r. The convergence histories of parameter RMS error for different cases are shown in Fig. 16. It is seen that with the higher level of noise the parameter RMS error, ε_p, reached the plateau region earlier. Although under the influence of 40% random noise, ε_p reduces to a relatively high value, the reconstructed solution visually matches the exact solution quite well as shown in Fig. 17.

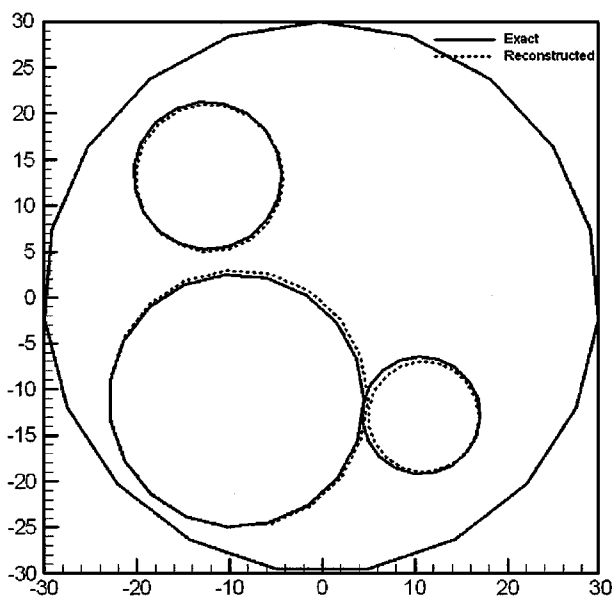

FIG. 17. Comparison between exact and reconstructed solutions of 40% random noise for the three-circle case.

5. CONCLUSIONS

The present study has applied a boundary element method and a hybrid optimization method combing the genetic algorithm and the Powell method to solve the inverse problem of electrical impedance tomography. A Pareto multiobjective approach was applied to better use the spatial information in the optimization procedure and to enhance the convergence speed.

Comparisons were made between a GA and a calculus-based Powell optimization method for 2D and 3D problems from simple to more complex cases. The genetic algorithms showed the ability to converge robustly to the correct solution in all 2D and 3D problems considered in the present study. However, the genetic algorithm required a much higher number of forward problem solutions and was much slower than the Powell method. The hybrid scheme combining the Powell method and the genetic algorithm significantly improved the convergence speed and was very robust even in the most complex cases we tested.

With a point parameterization method, the current scheme was found to be successfully applicable to reconstruct highly irregular internal objects. Despite less than the perfect match, the overall characteristics were well captured. By adding an extra on/off parameter, the current scheme was also successfully applied to reconstruct the image without a priori knowledge of the exact number of internal objects.

The study of the influence of noise showed that the current scheme is robust in the presence of noise for the cases tested. This implies that it may still work well when the experimentally measured data is of low accuracy.

ACKNOWLEDGMENTS

We acknowledge helpful discussions with many colleagues at Dynaflow, Inc. This study was supported by a National Science Foundation Small Business Innovation research program via Grants DMI-9461681 and DMI-9806707, and by internal Dynaflow, Inc. IR&D funds.

REFERENCES

1. O. C. Jones, J-T. Lin, H. Shu, L. Ovacik, and Y. He, Impedance imaging relative to binary mixtures, in *Symposium on Liquid Solid Flows* (ASME FED, New York, 1994), Vol. 189.
2. T. J. O'Hern, J. R. Torczynski, S. L. Ceccio, A. L. Tassin, G. L. Chahine, R. Duraiswami, and K. Sarkar, Development of an electrical impedance tomography system for an air–water vertical bubble column, in *Forum on Measurement Techniques in Multiphase Flows* (ASME FED, New York, 1995), Vol. 233, p. 531.
3. R. C. Waterfall, R. He, and C. M. Back, Visualizing combustion using electrical impedance tomography, *Chem. Eng. Sci.* **52**, No. 13, 2129 (1997).
4. A. M. Dijkstra, B. H. Brown, and A. D. Leathard, Clinical applications of electrical impedance tomography, *J. Med. Eng. Tech.* **17**, No. 3, 89 (1993).
5. T. J. Yorkey, J. G. Webster, and W. J. Tompkins, Comparing reconstruction algorithms for electrical impedance tomography, *IEEE Trans. Biomed. Eng.* **BME-34**, No. II (1987).
6. E. J. Woo, P. Hua, and W. J. Tomkins, Finite-element method in electrical impedance tomography, *Med. Biol. Eng. Comput.* **32**, No. 5, 530 (1994).
7. R. Duraiswami, K. Sarkar, S. Prabhukumar, and G. L. Chahine, Boundary element techniques for efficient 2D and 3D electrical impedance tomography, *Chem. Eng. Sci.* **52**, 2185 (1997).
8. R. Duraswami, K. Sarkar, and G. L. Chahine, Efficient 2D and 3D electrical impedance tomography using dual reciprocity boundary element techniques, *Eng. Anal. Boundary Elements* **22**, 13 (1998).

9. N. A. Gumerov and G. L. Chanine, Singular BEM and its application to 3D electrical impedance tomography, in *13th ASCE EMD Conference Proceedings, Baltimore, June 1999.*
10. N. A. Gumerov, G. L. Chanine, and A. G. Goumilevski, The dipole approximation method and its coupling with the regular boundary element method for efficient impedance tomography, in *13th International Conference on Boundary Element Technology, BETECH'99 Las Vegas, June 1999.*
11. J. H. Holland, Genetic algorithms, *Scientif. Am.* 44 (1975).
12. D. E. Goldberg, *Genetic Algorithms in Search, Optimization & Machine Learning* (Addison–Wesley, Reading, MA, 1989).
13. F. Y. Cheng and D. Li, Genetic algorithm development for multiobjective optimization of structures, *AIAA J.* **36**, 1105 (1998).
14. G. L. Chahine, N. A. Gumerov, C.-T. Hsiao, and A. G. Goumilevski, *BEM Methods for Efficient 2D and 3D Electrical Impedance Tomography*, NSF Phase II SBIR Final Report. [Also, Dynaflow, Inc. Technical Report 96008-1 (August 1998)]
15. G. L. Chahine, T. O. Perdue, and C. B. Tucker, *Interaction between Underwater Explosion Bubble and a Solid Submerged Body*, Dynaflow, Inc. Technical Report 89001-1, (August 1989).
16. D. K. Han and A. Prosperetti, A shape decomposition technique in electrical impedance tomography, *J. Comput. Phys.* **155**, 75 (1999).
17. W. H. Press, S. A. Teukolsky, W. T. Vetterling, and B. P. Flannery, *Numerical Recipes*, 2nd ed. (Cambrige Univ. Press, Cambridge, UK, 1992).
18. F. S. Acton, *Numerical Methods That Work* (Mathematical Association of America, Washington, DC, 1970) p. 464. [1990 corrected edition]
19. M. E. Alexander and R. L. Somorjai, The registration of MR images using multiscale robust methods, *Magn. Reson. Imag.* No. 5, 453 (1996).
20. R. Bähring, D. Bowie, M. Benveniste, and M. L. Mayer, Permeation and block of rat GluR6 glutamate receptor channels by internal and external polyamines, *J. Physiol.* **502**, No. 3, 575 (1997).
21. J. F. Kinkel and M. Thomas, Estimation of vehicle dynamic and static parameters from magnetometer data, *J. Guidance, Control, Dynam.* **20**, No. 1, 111 (1997).
22. J. Oksanen, Why the beta-function cannot be used to estimate skewness of species responses, *J. Veg. Sci.* **8**, 147 (1997).
23. R. P. Brent, in *Algorithms for Minimization without Derivatives* (Prentice Hall International, Englewood Cliffs, NJ, 1973), Chap. 7.
24. J. E. Dennis, Jr. and R. B. Schnable, *Numerical Methods for Unconstrained Optimization and Nonlinear Equations* (Prentice Hall International, Englewood Cliffs, NJ, 1983).